Effect of Acid Predissolution on Fibril Size and Fibril Flexibility of Synthetic β-Amyloid Peptide

Chih-Lung Shen,* Michael C. Fitzgerald,‡ and Regina M. Murphy*
Departments of *Chemical Engineering and ‡Chemistry, University of Wisconsin, Madison, Wisconsin 53706 USA

ABSTRACT β-amyloid peptide (Aβ) is the major protein component of senile plaques and cerebrovascular amyloid deposits in Alzheimer's patients. Several researchers have demonstrated that Aβ is neurotoxic in in vitro and in vivo systems. Peptide aggregation state and/or conformation might play a significant role in determining the toxicity of the peptide. The size and flexibility of fibrils formed from the synthetic peptide β(1–39), corresponding to the first 39 residues of Aβ, were determined. Samples were prepared either directly from lyophilized peptide or diluted from a 10 mg/ml stock solution in 0.1% trifluoroacetic acid (TFA). All samples had a final peptide concentration of 0.5 mg/ml, a final pH of 7.4, and a final NaCl concentration of 0.14 M. The molecular weight and linear density of the fibrils increased with increasing pre-incubation time in TFA, based on static light scattering measurements. Analysis of the angular dependence of the intensity of scattered light indicated that the fibrils were semi-flexible chains and that the fibril flexibility decreased with increasing pre-incubation time in TFA. There was a concomitant change in phase behavior from precipitation to gelation with the decrease in fibril flexibility.

INTRODUCTION

β-amyloid peptide (Aβ) is the major protein component of senile plaques and cerebrovascular amyloid deposits from Alzheimer's patients (Glenner and Wong, 1984; Wong et al., 1985; Masters et al., 1985). Aβ is a proteolytic product of a membrane-associated precursor protein and contains both extracellular and transmembrane residues of the precursor (Kang et al., 1987; Haass and Selkoe, 1993). The naturally occurring peptide has 39–43 residues and displays both N- and C-terminal heterogeneity (Masters et al., 1985; Prelli et al., 1988).

Deposition of Aβ in the form of amyloid fibrils is a defining characteristic of Alzheimer's disease. Soluble forms of Aβ are secreted by some cultured cells and have been detected in cerebrospinal fluid and in plasma (Haass et al., 1992; Seubert et al., 1992; Shoji et al., 1992). Aβ might play a significant role in the onset and/or progression of the disease (Joachim and Selkoe, 1992; Rosenberg, 1993). A number of experiments have shown that the peptide can exert considerable neurotrophic and/or neurotoxic effects in vitro (e.g., Whitson et al., 1989; Yankner et al., 1990; Busciglio et al., 1993; Loo et al., 1993). In some cases, Aβ was not directly toxic, but rather increased the susceptibility of the cells to injury from glutamate (Koh et al., 1990; Mattson et al., 1992). Results from in vivo experiments have been somewhat contradictory. Some researchers have reported neurotoxic effects or tissue damage caused by injection of amyloid cores or synthetic peptides (Frautschy et al., 1991; Kowall et al., 1991; Emre et al., 1992; Kowall et al., 1992), whereas other reports show no in vivo toxic effect (Clemens et al., 1992; Games et al., 1992; Podlisny et al., 1992; Stein-Behrens et al., 1992).

The extent of aggregation and/or the conformational state may critically influence the degree of toxicity (Pike et al., 1991a, b, 1993; Busciglio et al., 1992; Simmons et al., 1994). Toxicity can depend on the source of the peptide (Busciglio et al., 1992; May et al., 1992). Thus, proper assessment of the biological activity of Aβ may require detailed knowledge of the physical properties of the peptide in solution.

Some synthetic peptides homologous to Aβ have limited solubility at physiological pH and ionic strength (Hilbich et al., 1991; Burdick et al., 1992). This has led a number of researchers to prepare stock solutions of Aβ in a variety of solvents before dilution into cell cultures in their toxicity assays, sometimes with dramatically different results depending on the solvent used (Mattson et al., 1992; Waite et al., 1992). However, little is known about the effect of solvents on the aggregation characteristics of the peptide.

In this report, we investigated the effect of predissolving the synthetic peptide β(1–39) in 0.01 M phosphate buffer or 0.1% trifluoroacetic acid (TFA) before preparing solutions at physiological pH and ionic strength. Changes in chemical composition, secondary structure, fibril structure, and fibril-fibril aggregation were probed using mass spectroscopy, circular dichroism, and fluorescence spectroscopy, and dynamic and static light scattering. Minor changes in sample preparation resulted in significant differences in the fibril size, fibril flexibility, and phase separation behavior. These changes in fibril characteristics were not accompanied by measurable changes in chemical composition or secondary structure.

Received for publication 5 April 1994 and in final form 31 May 1994.

Address reprint requests to Dr. Regina M. Murphy, Department of Chemical Engineering, University of Wisconsin, 1415 Johnson Drive, Madison, WI 53706. Tel.: 608-262-1587; Fax: 608-262-5434.

Abbreviations used: Aβ, β-amyloid peptide; DLS, dynamic light scattering; DTT, dithiothreitol; HPLC, high pressure liquid chromatography; MALDI, matrix-assisted laser desorption-ionization mass spectroscopy; PBSA, phosphate-buffered saline with azide; SLS, static light scattering; TFA, trifluoroacetic acid.

0006-3495/94/09/1238/09 $2.00

MATERIALS AND METHODS

Peptide synthesis and purification

The peptide β(1–39) was synthesized and purified by Nuros, Inc. (San Jose, CA). The peptide sequence, taken from Kang et al. (1987), is DAEFRHDSGYEVHHQKLVFFAEDVGSNKGAIIGLMVGGV. The peptide was purified by reverse-phase HPLC. Purity was reported as greater than 95%.

Circular dichroism spectroscopy

β(1–39) solutions were prepared in 0.1% TFA (Sigma, St. Louis, MO) or by dilution of a stock solution of 10 mg/ml peptide in 0.1% TFA into 0.01 M potassium phosphate buffer, pH 7.6. Final peptide concentration was 0.2 mg/ml. The peptide solutions were filtered through a 0.45 μm Millipore filter (Bedford, MA) to remove dust and then placed into a vacuum system to degas. Circular dichroism spectra in the far-UV (190–240 nm) were obtained using a modified Cary Model 60 spectropolarimeter (On-line Instrument Systems, Bogart, GA). A 0.1 cm quartz cell was used for measurements. The instrument was calibrated using d(+)-10-camphorsulfonic acid. The spectral measurements were taken approximately 3 h after sample preparation. Ten scans of the blank were measured and averaged as a baseline. Ten runs of each spectrum were measured from which the baseline was subtracted. The secondary structure was calculated from mean ellipticities using the standard secondary structural parameters given by Chang et al. (1978).

Fluorescence measurements

Fluorescence spectra for β(1–39) were obtained on a Model M-3 Alphascan (Photon Technology International, South Brunswick, NJ) spectrofluorimeter. The concentration of β(1–39) was 0.5 mg/ml in 0.1% TFA. The sample was incubated in a 1 × 0.4 cm^2 cuvette at a temperature of 25 ± 0.1°C. Fluorescence emission spectra from 285 to 500 nm were measured 3 times and averaged, using excitation at 275 nm. Data were collected from 5 min to 1 day after sample preparation.

Electron microscopy

A drop of the peptide solution was placed on a pioloform-coated 300-mesh electron microscope copper grid. After blotting, a drop of 1% ammonium molybdate was placed on the grid while it was held with fine forceps. The grid was blotted on filter paper and allowed to dry before observing the specimen in a JEOL (Peabody, MA) 100CX Electron Microscope at 60 kV.

High-performance liquid chromatography (HPLC)

HPLC experiments were performed using the Waters (Millipore, Milford, MA) Model 625 LC system and the Waters Protein-PAK 125 column. The mobile phase was 0.1% TFA at a flow rate of 1 ml/min. Ten μl of 10 mg/ml β(1–39) in 0.1% TFA was injected. Elution peaks were detected by absorbance at 280 nm. The column was calibrated with ovalbumin (43 kDa), myoglobin (17 kDa), ribonuclease A (14 kDa), and insulin (5.7 kDa) (all from Sigma).

Matrix-assisted laser desorption-ionization mass spectroscopy (MALDI)

MALDI mass spectrometry was performed using a Vestec Model VT 2000 (Houston, TX) laser desorption linear (2 m) time-of-flight mass spectrometer modified with a 24 sample loading system combined with video camera viewing. Desorption/ionization of the sample was accomplished with a Lumonics (Warwickshire, England) Model HY 400 ND:YAG laser frequency tripled to 355 nm. The laser pulse width was 10 ns, and the pulse frequency was 10 Hz. Ions were accelerated in one stage through a potential of 30 keV in the source region and detected by a 20 stage focused mesh electron multiplier (Becton-Dickinson Model MM1–1SG) at the end of the flight tube. A particle guide made of nickel wire (0.12 mm in diameter) also spanned the length of the 2 m flight path, and was biased at 120 V so ions were efficiently transported along the center axis of the flight tube. All spectra were obtained using the matrix alpha-cyano-4-hydroxycinnamic acid (Aldrich, Milwaukee, WI) in the positive ion mode and summed over 50 laser shots. Time to mass conversion was accomplished using insulin (MW = 5733.5 Da) as an internal standard.

Saturated matrix solutions were prepared fresh daily in 50/50 acetonitrile/water. Lyophilized β(1–39) was dissolved in pure water, 0.1% TFA, or 0.5% TFA to give an analyte concentration of 10 μM. Typically, 5 μl of saturated matrix solution was mixed with 1 μl of analyte solution and 1 μl of an aqueous insulin solution (10 μM) before deposition of 2 μl of this mixture on a stainless steel probe tip. The solvent was allowed to evaporate at room temperature before insertion into the source region of the mass spectrometer.

Static light scattering

All aqueous buffers were double-filtered through a 0.22-μm filter (Millipore, Bedford, MA) before use. All samples had a final peptide concentration of 0.5 mg/ml, a final pH of 7.4, and a final salt concentration of 0.01 M K_2HPO_4/KH_2PO_4 and 0.14 M NaCl. A summary of the sample preparation methods is shown in Table 1. Sample A was made by dissolving 0.5 mg of lyophilized peptide into 0.5 ml of 0.01 M phosphate buffer containing 0.02% (w/v) sodium azide, then diluting with 0.5 ml of 0.01 M phosphate buffer, 0.28 M NaCl, and 0.02% (w/v) sodium azide. The pH was adjusted to 7.4 with 0.5 N NaOH. Samples B, C, and D were prepared from stock solutions of β(1–39) at 10 mg/ml in 0.1% TFA that were allowed to stand at room temperature for 5 min, 1 h, and 1 day, respectively, and then diluted into phosphate buffered saline (PBSA: 0.01 M K_2HPO_4/KH_2PO_4, 0.14 M NaCl, 0.02% (w/v) sodium azide) to a final concentration of 0.5 mg/ml and a final pH of 7.4. Sample E was prepared to exclude any possibility of oxidation. β(1–39) at 10 mg/ml was made by dissolving 0.5 mg of lyophilized peptide in the presence of 0.5 mg of dithiothreitol (DTT, Sigma) in 50 μl of 0.1% oxygen-free TFA, which was sparged with helium at a flow rate of 100 ml/min for 1 h before use. The sample was stored in a 1.5 ml Ependorff tube that had been sparged with nitrogen, sealed by parafilm, and incubated for 1 day at 25°C. The stock solution was then diluted into PBSA to give a final peptide concentration of 0.5 mg/ml at pH 7.4. All samples were filtered with a 0.45-μm filter (Millipore) and transferred into a pre-cleaned 8 mm o.d. cylindrical light scattering cell (Hellma, Jamaica, NY). The concentration of some samples was checked using a Hitachi Model U-2000 UV-Vis spectrophotometer (Hitachi, Chicago, IL) before and after filtration; there was no significant loss in absorbance at 280 nm due to filtration.

TABLE 1 Summary of sample preparation methods

Sample	Initial stock solution	Preincubation time in stock solution	Final solution
A	1 mg/ml β(1–39) in 0.01 M phosphate	1 min	0.5 mg/ml β(1–39) in PBSA
B	10 mg/ml β(1–39) in 0.1% TFA	5 min	Same as Sample A
C	Same as Sample B	1 h	Same as Sample A
D	Same as Sample B	1 day	Same as Sample A
E	10 mg/ml β(1–39) in He-sparged 0.1% TFA with 10 mg/ml DTT	1 day	Same as Sample A

Static light scattering (SLS) experiments were performed using a Malvern 4700c particle analyzer with a 128-channel autocorrelator (Malvern, Southborough, MA) and a Lexel Model 95–2 argon-ion laser (Lexel Laser Inc., Fremont, CA) equipped with an etalon. The laser was operated at a power of 75–200 mW and at a wavelength of 488 nm. The laser beam was focused onto the scattering cell. The entire assembly was leveled and fixed on an optical table (Technical Manufacturing Co., Brockton, MA). The scattering cell was placed in a temperature-controlled bath containing the refractive index matching fluid decahydronaphthalene (Aldrich, Milwaukee, WI), which has a refractive index of 1.479. The temperature was controlled to 25 ± 0.1°C using a circulating water bath (VWR, Chicago, IL). To reduce stray light, the equipment was enclosed in a black box.

The scattered light intensity $I_s(\theta)$ was collected for 12 s at 22 different angles between 20° and 140°. Each measurement was repeated 10 times and then averaged. The scattered light intensity of the background and solvent contributions $I_b(\theta)$ was then measured at the same conditions. The results were normalized with respect to intensity data $I_t(\theta)$ from spectrophotometric grade toluene (Aldrich) to obtain the Rayleigh ratio $R_s(q)$.

For macromolecules, static light scattering data are commonly represented by

$$\frac{Kc}{R_s(q)} = \frac{1}{P(q)\langle M\rangle_w} + 2Bc + \cdots, \tag{1}$$

where c is the concentration of sample (g/ml), $\langle M\rangle_w$ is the weight-averaged molecular weight of the particles in solution, $P(q)$ is a particle scattering factor, $K = 4\pi^2 n^2 (dn/dc)^2 / N_A \lambda_o^4$, dn/dc is the refractive index increment, N_A is Avogadro's number, λ_o is the wavelength of the light in vacuo, and B is the second virial coefficient. For determination of dn/dc, solutions of peptide were made at known concentrations and the refractive index of the solution was measured using a Milton-Roy (Rochester, NY) Abbe-3L refractometer. The refractive index increment was determined to be 0.112 ml/g.

For our system, K was assumed to be independent of the state of aggregation. At low concentrations and low angles (low q), Eq. 1 can be rewritten as

$$\frac{Kc}{R_s(q)} = \frac{1}{\langle M\rangle_{w,app}}\left(1 + \frac{1}{3}q^2\langle R_g^2\rangle_{z,app}\right), \tag{2}$$

where q is the scattering vector ($=4\pi n/\lambda_o \sin(\theta/2)$), $\langle M\rangle_{w,app}$ is the apparent weight-averaged molecular weight, and $\langle R_g^2\rangle_{z,app}$ is the light-scattering-averaged squared radius of gyration.

For particles with dimensions similar to the wavelength of the incident light, the angular dependence of the scattered intensity can be used to obtain information on the shape of the particles in solution. The scattering factor $P(q)$ can be evaluated from the intensity data over the entire range of q from

$$P(q) = \left(\frac{R_s(q)}{Kc\langle M\rangle_{w,app}}\right). \tag{3}$$

The theoretical scattering factor $P(q)$ for semi-flexible chains is given by (Koyama, 1973)

$$P(q) = \frac{2}{L_c^2}\int_0^{L_c} (L_c - t)\cdot \exp\left(-\frac{1}{6}q^2 \cdot l_k \cdot tf(t)\right) \times \frac{\sin(q\cdot tg(t))}{q\cdot tg(t)}\,dt, \tag{4}$$

where L_c is the contour length and l_k is the Kuhn statistical segment length, which is equal to 2 times the persistence length L_p. The functions $tf(t)$ and $tg(t)$ are

$$tf(t) = \frac{\langle r^2\rangle}{l_k} - \frac{t^2 g(t)^2}{l_k}$$
$$t^2 g(t)^2 = \langle r^2\rangle\left(\frac{5}{2}\left(1 - \frac{3}{5}K\right)\right)^{1/2} \qquad K = \frac{\langle r^4\rangle}{\langle r^2\rangle^2}. \tag{5}$$

The moments $\langle r^2\rangle$ and $\langle r^4\rangle$ are given as (Benoit and Doty, 1953)

$$\langle r^2\rangle = \frac{l_k^2 x}{2} - \frac{l_k^2}{2}(1 - e^{-x})$$
$$\langle r^4\rangle = l_k^4\left[\frac{5}{12}x^2 - \frac{13}{9}x - \frac{1}{54}(1 - e^{-3x}) + 2(1 - e^{-x}) - \frac{1}{2}xe^{-x}\right], \tag{6}$$

where $x = 2t/l_k$.

The mean square radius of gyration $\langle R_g^2\rangle$ of a semi-flexible chain can be evaluated from (Benoit and Doty, 1953)

$$\langle R_g^2\rangle = \frac{L_c l_k}{6} - \frac{l_k^2}{4} + \frac{l_k^3}{4L_c} - \frac{l_k^4}{8L_c^2}(1 - e^{(-2L_c/l_k)}). \tag{7}$$

The scattered intensity data were plotted as $Kc/R_s(q)$ vs. q^2 and fit by weighted least-squares regression to a straight line at the low angles. From the slope and intercept, $\langle R_g^2\rangle_{z,app}$ and $\langle M_g^2\rangle_{w,app}$ were determined along with SDs. Light scattering data were plotted as $q^2P(q)$ vs. q or as $qP(q)/\pi$ vs. $q\langle R_g^2\rangle_{z,app}^{1/2}$ (Schmidt et al., 1985). These formats are known as Kratky and Holtzer plots, respectively. Eqs. 4–6 were fit by inspection to the Kratky and Holtzer plots to determine L_c and l_k.

Dynamic light scattering

Dynamic light scattering (DLS) experiments were conducted using the same apparatus and samples as used for SLS experiments. The scattered light intensity was collected at 90° from the transmitted beam and converted to the normalized first-order electric field autocorrelation function $g^{(1)}(\tau)$, where τ is the decay time. Data were collected for 20 runs for 30 s duration each time and then averaged. Data were analyzed using the method of cumulants, by fitting to the third-order cumulants expression

$$\ln|g^{(1)}(\tau)| = -\langle\Gamma\rangle\tau + \frac{1}{2!}\mu_2\tau^2 - \frac{1}{3!}\mu_3\tau^3 + \cdots, \tag{8}$$

where $\langle\Gamma\rangle$ is the initial decay rate, and μ_2 and μ_3 are the second and third moments, respectively. $\langle\Gamma\rangle^{-1}$ can be considered a relaxation time, corresponding to the time scale for motion of the particles in solution. $\langle\Gamma\rangle$ is related to the apparent z-average translational diffusion coefficient by

$$\langle D\rangle_{z,app} = \frac{\langle\Gamma\rangle}{q^2}, \tag{9}$$

where the particle shape factor, internal motions, and intermolecular interactions are not accounted for. An apparent hydrodynamic radius $\langle R_h\rangle_{app}$ can be calculated from the Stokes-Einstein equation:

$$\langle R_h\rangle_{app} = \frac{k_B T}{6\pi\eta_s\langle D\rangle_{z,app}}, \tag{10}$$

where k_B is the Boltzmann constant, T is the absolute temperature, and η_s is the solvent viscosity.

For semi-flexible chains, the hydrodynamic radius R_h can be calculated using equations derived by Yamakawa and Fujii (1973). For chains that have $L_c/l_k > 2.278$, the hydrodynamic radius is given as

$$\frac{1}{2}\frac{L_c}{R_h} = A_1\left(\frac{L_c}{l_k}\right)^{0.5} + A_2 + A_3\left(\frac{L_c}{l_k}\right)^{-0.5} + A_4\left(\frac{L_c}{l_k}\right)^{-1} + A_5\left(\frac{L_c}{l_k}\right)^{-1.5}. \tag{11}$$

For $L_c/l_k \le 2.278$,

$$\frac{1}{2}\frac{L_c}{R_h} = C_1\ln\left(\frac{L_c}{d}\right) + C_2 + C_3\left(\frac{L_c}{l_k}\right) + C_4\left(\frac{L_c}{l_k}\right)^2 + C_5\left(\frac{L_c}{l_k}\right)^3 + C_6\left(\frac{d}{L_c}\right)\ln\left(\frac{L_c}{d}\right) + C_7\left(\frac{d}{L_c}\right) + C_8\left(\frac{d}{L_c}\right)^2 + C_9\left(\frac{d}{L_c}\right)^3 + C_{10}\left(\frac{d}{L_c}\right)^4, \tag{12}$$

where d is the hydrodynamic diameter of the chain, and the coefficients A_i and C_i are given by Yamakawa and Fujii (1973).

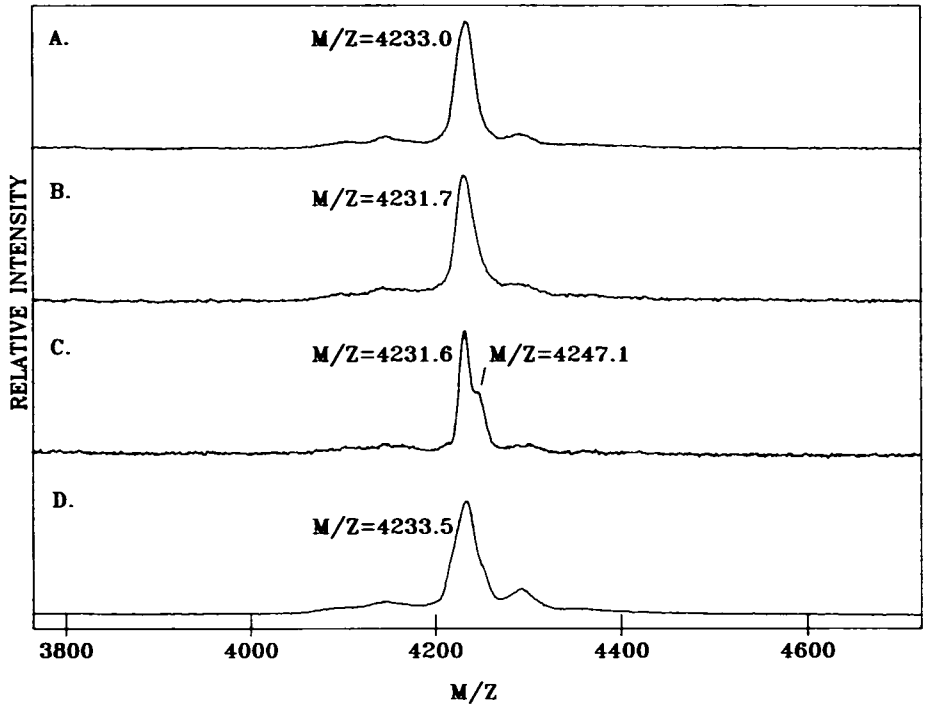

FIGURE 1 Mass spectra for (*A*) β(1–39) in water for 20 min, (*B*) β(1–39) in 0.5% TFA for 20 min, (*C*) β(1–39) in 0.5% TFA for 24 h, and (*D*) β(1–39) in 0.5% TFA with 0.8 M 2-mercaptoethanol for 24 h.

RESULTS

Oxidization of β(1–39) in TFA

MALDI spectra for β(1–39) in both pure water and 0.5% TFA were taken immediately after sample preparation; results are shown in Fig. 1, *A* and *B*, respectively. Intense signals at *M/Z* = 4233.0 (Fig. 1 *A*) and 4231.7 (Fig. 1 *B*) were observed, consistent with the calculated molecular mass of 4232 for monomeric β(1–39). Virtually identical spectra were obtained for β(1–39) in 0.1% TFA immediately after sample preparation, and for β(1–39) in 0.1% TFA 24 h after sample preparation (data not shown). The spectrum for β(1–39) in 0.5% TFA for 24 h after sample preparation is shown in Fig. 1 *C*. An intense signal for the singly charged peptide at the appropriate molecular mass was observed. In addition, a significant high molecular mass shoulder at *M/Z* = 4247.1 was detected. The sample in Fig. 1 *C* was treated with 0.8 M 2-mercaptoethanol for 48 h, and a spectrum was obtained (Fig. 1 *D*). The high molecular mass shoulder disappeared, although the peak width was greater than in Fig. 1 *B*. Based on these results, no degradation or change in chemical composition occurs after one day in 0.1% TFA or water. The data suggest that the peptide is partially oxidized after 24 h in 0.5% TFA, presumably at Met-35.

Secondary structure

Circular dichroism spectra are shown in Fig. 2. Two samples were prepared by dilution of a stock peptide solution in 0.1% TFA into phosphate buffer. The samples were incubated for different lengths of time in TFA before dilution. For both samples, analysis of the spectra indicated a content of approximately two-thirds β-sheet and one-third random coil. This result was independent of the time period of incubation of β(1–39) in 0.1% TFA. The spectrum of the peptide in 0.1% TFA was considerably different than that of the peptide in phosphate buffer. In 0.1% TFA, β(1–39) contained approximately one-third β-sheet, one-fourth β-turn, with the remainder random coil.

The fluorescence emission spectrum of β(1–39) in 0.1% TFA was measured with excitation at 275 nm. An emission maximum was observed at 302 nm (data not shown), which is characteristic of tyrosine emission (Jordano et al., 1983). Fluorescence emission was followed for 5 min to 24 h after sample preparation. Tyrosine fluorescence is partially

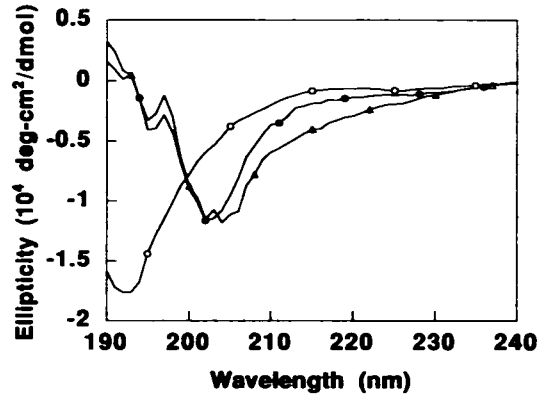

FIGURE 2 Circular dichroism spectra for β(1–39). 10 mg/ml β(1–39) dissolved in 0.1% TFA for 5 min then diluted into 0.01 M phosphate buffer, pH 7.6 (△), 10 mg/ml β(1–39) dissolved in 0.1% TFA for 3 months then diluted into phosphate buffer (●), and β(1–39) in 0.1% TFA (○). Final peptide concentration for all samples was 0.2 mg/ml. Spectra were obtained 3 h after sample preparation.

quenched when hydrogen bonded with water and totally quenched when hydrogen bonded with a carbonyl oxygen (Cowgill, 1976). There was no change in the fluorescence spectra or in the peak intensity as a function of time (data not shown). This indicates that there was no measurable change in the tyrosine residue environment under the experimental conditions.

Size exclusion HPLC

For 10 mg/ml β(1–39) in 0.1% TFA, with 0.1% TFA as the mobile phase, the HPLC chromatogram showed a single sharp peak. Based on calibration of the column, this corresponded to an apparent molecular mass of approximately 6 kDa (data not shown). No significant change was detected when the sample was injected one day after preparation. These results show that the peptide is dissociated, probably into monomers, in 0.1% TFA.

Confirmation of presence of amyloid fibrils

Peptide solutions prepared either directly by dissolution of lyophilized peptide into phosphate buffer, or by dissolution of lyophilized peptide in 0.1% TFA followed by dilution into PBSA both showed a red shift in the absorbance spectra of Congo red (data not shown), characteristic of amyloid fibrils (Klunk et al., 1989). Electron micrographs showed that the peptide formed fibrillar structures with an apparent diameter of approximately 10 nm. Representative micrographs of Samples B and D, taken several days after sample preparation, are shown in Fig. 3.

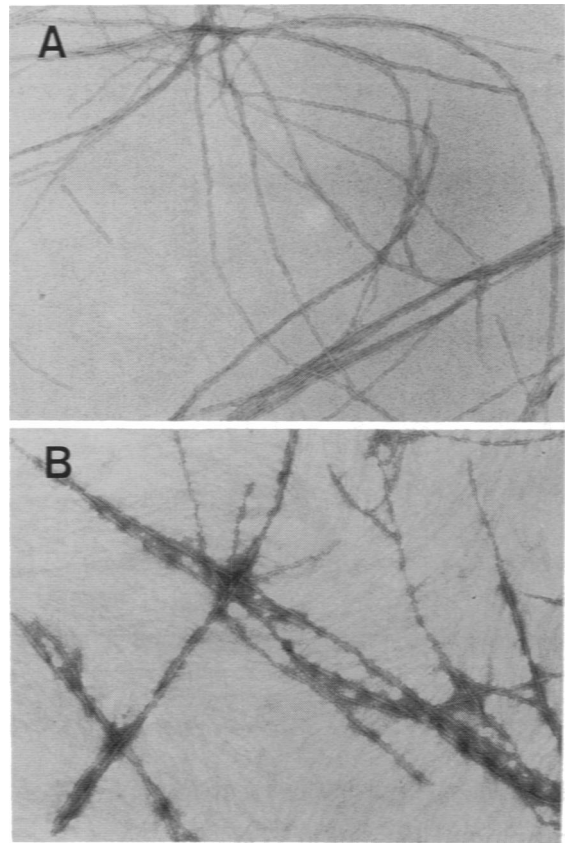

FIGURE 3 Electron micrographs of peptide solutions at 24,500× magnification, taken several days after sample preparation. (*A*) Sample B, incubated for 5 min in 0.1% TFA before dilution into PBSA. (*B*) Sample D, incubated for 1 day in 0.1% TFA before dilution into PBSA. Sample preparation is described in more detail in Materials and Methods and in Table 1.

Characterization of fibril size and structure by light scattering

Samples A to D were analyzed by static light scattering. The data were collected 12 h after dilution into PBSA. Intensity data were plotted as $Kc/R_s(q)$ vs. q^2 in Fig. 4. Because aggregation is concentration-dependent, experiments at multiple concentrations could not be performed and analyzed using a conventional Zimm plot. Equation 2 was used to analyze the data for values of $q^2\langle R_g^2\rangle_{z,app} < 4$. This limit was chosen because $P(q)^{-1}$ is fairly independent of particle shape for values of $q^2\langle R_g^2\rangle_{z,app} < 4$ (Benoit and Doty, 1953). $\langle R_g^2\rangle_{z,app}$ was obtained from the slope of the plot at low q to satisfy the aforementioned limit. $\langle M\rangle_{w,app}$ was calculated from the intercept of $Kc/R_s(q)$ vs. q^2. Results are shown in Table 2. $\langle M\rangle_{w,app}$ for Samples A and B were not significantly different. In contrast, $\langle M\rangle_{w,app}$ increased with increasing preincubation time in 0.1% TFA (Samples C and D).

By recasting the data in a different form, structural information was obtained (Schmidt et al., 1985). $P(q)$ was calculated from the data using Eq. 3 and the value of $\langle M\rangle_{w,app}$ listed in Table 2. Intensity data were replotted as $q^2P(q)$ vs. q in Fig. 5 and as $qP(q)/\pi$ vs. $q\langle R_g^2\rangle_{z,app}^{1/2}$ in Fig. 6. These formats are known as Kratky and Holtzer plots, respectively. For flexible chains, a definite plateau appears in the Kratky plot (Fig. 5); the height of the plateau corresponds to $12/L_c l_k$. For stiff, rodlike chains, no definite plateau emerges. In the Holtzer plot (Fig. 6), the asymptotic value at large q $\langle R_g^2\rangle_{z,app}^{1/2}$ corresponds to $1/L_c$. A maximum appears at intermediate values of $q\langle R_g^2\rangle_{z,app}^{1/2}$ for chains with some flexibility, whereas for rods there is no internal maximum. The ratio of the maximum to the asymptotic value (at large q) of $qP(q)/\pi$ is proportional to the number of segments N_k, where $N_k = L_c/l_k$. The stiffer the chain, the lower the value of N_k. The position of the maximum indicates the degree of polydispersity, U, which is a measure of $\langle M\rangle_w/\langle M\rangle_n$, where $\langle M\rangle_n$ is the number-averaged molecular weight.

Theoretical curves for $P(q)$ as a function of L_c and l_k were generated from Eqs. 4–6 and compared with the experimental data. The best fit determination of L_c and l_k was made by visual inspection. The calculated curves for $P(q)$ are shown along with the data in Figs. 5 and 6. The chosen fit to the experimental data is shown as a solid line in Figs. 5 and 6, and the chosen values of L_c and l_k are included in Table 3. In Figs. 5 and 6, most of the experimental data were included in the region between the two dotted curves that were computed using $L_c \pm 100$ nm and $l_k \pm 10$ nm for Samples A, B, and C, and $L_c \pm 50$ nm and $l_k \pm 10$ nm for Sample D. The

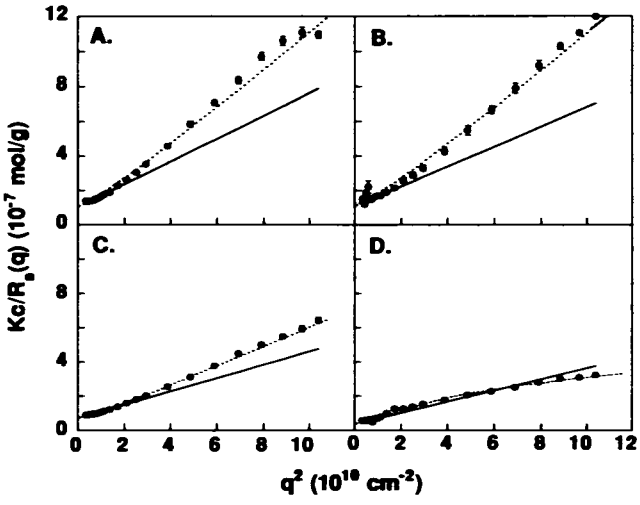

FIGURE 4 $Kc/R_s(q)$ vs. q^2 for 0.5 mg/ml β(1–39) in PBSA, pH 7.4. Sample A was made directly from lyophilized peptide. Samples B, C, and D were made from 10 mg/ml β(1–39) that was incubated in 0.1% TFA for 5 min, 1 h, and 1 day, respectively, before dilution into PBSA. Sample preparation is described in more detail in Materials and Methods and in Table 1. Open circles show experimental data. Error bars show the SD for intensity measurements at each angle. The data were fit using the structure factor of the flexible chain (Eqs. 4–6, - - - -). $\langle M\rangle_{w,app}$ and $\langle R_g^2\rangle_{z,app}$ were determined from the slope and intercept of the solid line, which represents the fit of the data to Eq. 2.

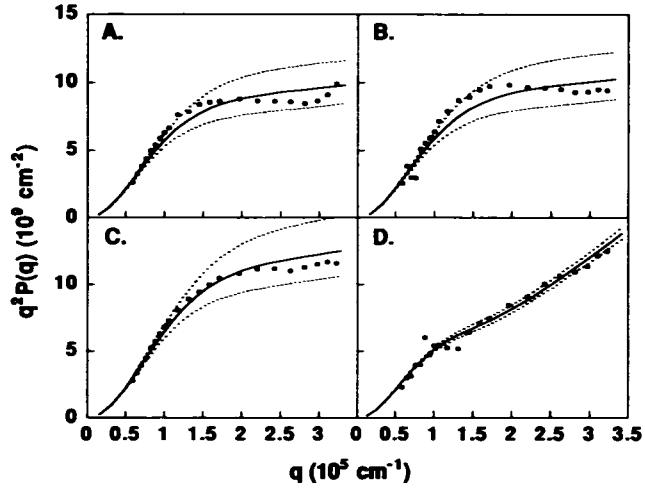

FIGURE 5 Kratky plots for Samples A, B, C, and D. Open circles show experimental data points; dotted lines represent the calculated curves for $P(q)$ from Eq. 4 using different intervals of ~3–10% of L_c and l_k; solid line represents the best fit of the data to Eq. 4.

TABLE 2 Summary of SLS and DLS results

Sample	$\langle M\rangle_{w,app}$ (10^6 Da)	$\langle R_g^2\rangle_{z,app}^{1/2}$ (nm)	$\langle R_h\rangle_{app}$ (nm)
A	9.6 ± 0.4	138 ± 9	100
B	9.2 ± 0.6	128 ± 10	90
C	14.0 ± 0.5	128 ± 6	100
D	25.4 ± 4.0	159 ± 32	360

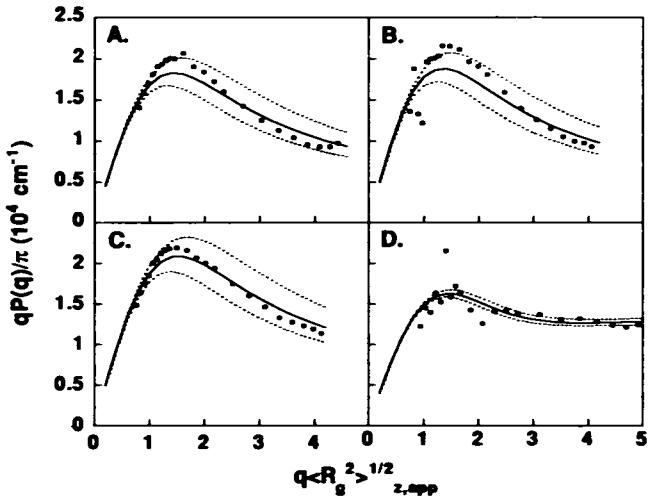

FIGURE 6 Holtzer plots for Samples A, B, C, and D. The same symbols are used as in Fig. 5.

theoretical radius of gyration was calculated from Eq. 7 using the values of L_c and l_k listed in Table 3. The calculated radius of gyration was consistent with the experimentally determined value (Table 2).

In Figs. 5 and 6, for Samples A to C, a clear plateau in the Kratky plot and a clear intermediate maximum in the Holtzer plot were present, indicative of a semi-flexible chain. In contrast, for Sample D, there was no clear plateau in the Kratky plot and only a very small intermediate maximum in the Holtzer plot, indicative of a stiffer structure. These qualitative observations are reflected in the values of l_k and N_k for the four samples. Specifically, the Kuhn length l_k is considerably greater, and the number of segments N_k is considerably smaller, for Sample D. The contour length L_c decreased with increasing pre-incubation time in 0.1% TFA.

An estimate of the degree of polydispersity U, as determined from the location of the maximum of the curves plotted in Fig. 6, is listed in Table 3. All samples have similar, relatively narrow polydispersities. The mass linear density M_L was calculated from $\langle M\rangle_{w,app}/L_c$. In addition, the apparent diameter d_{app} was calculated using the estimated hydrated specific volume V_h of β(1–39) of 1.11 cm^3/g (Kuntz and Kauzmann, 1974; Cohn and Edsall, 1943) and the equation

$$d_{app} = \left(\frac{4}{\pi}\frac{M_L \cdot V_h}{N_A}\right)^{0.5} \quad (13)$$

For Samples A and B, d_{app} is virtually the same. However, Sample D had a higher d_{app} than Samples A and B; Sample C had an intermediate d_{app}.

DLS measurements were taken on these samples, beginning 20 min after sample preparation and continuing for several days. The decay rate $\langle\Gamma\rangle$ at 90° vs. time for the first 48 h is plotted in Fig. 7. The initial value of $\langle\Gamma\rangle$ increased with increasing pre-incubation time in 0.1% TFA. However, the value of $\langle\Gamma\rangle$ at 48 h decreased with increasing pre-incubation time. There was a slight drop in $\langle\Gamma\rangle$ of Sample A over time.

TABLE 3 Summary of calculation results from Eqs. 4–7 and 11–12

Sample	L_c (nm)	l_k (nm)	M/L_c (10^3 Da/nm)	d_{app} (nm)	N_k	U	$\langle R_g^2 \rangle^{1/2}$ (nm)	R_h (nm)
A	1400	90	7	4	16	1.5	138	75
B	1400	85	7	4	16	1.4	135	74
C	1100	90	13	6	12	1.5	121	67
D	750	300	34	9	2.5	1.4	149	70

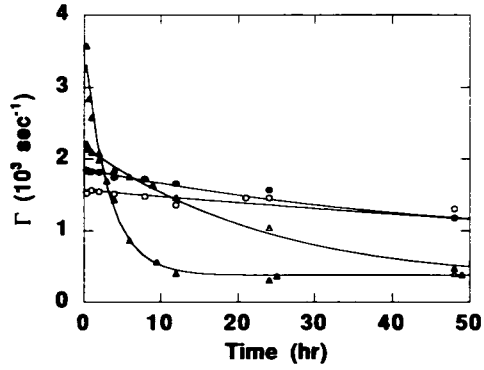

FIGURE 7 ⟨Γ⟩ vs. time for Samples A (○), B (●), C (△), and D (▲).

In contrast, ⟨Γ⟩ of Sample B decreased gently from 1850 to 1180 s^{-1}. ⟨Γ⟩ of Sample C dropped evenly from 2200 s^{-1} to 400 s^{-1}. ⟨Γ⟩ of Sample D decreased rapidly from 3580 to 500 s^{-1} at the first 10 h, then was about constant at 400 s^{-1}. The plot of ⟨Γ⟩ against t for Sample E was similar to Sample D (data not shown).

$\langle R_h \rangle_{app}$ was calculated from ⟨Γ⟩ for the data taken at 12 h after sample preparation using Eqs. 9–10. Results are shown in Table 2. The theoretical hydrodynamic radius was calculated from Eqs. 11 and 12 using the values of L_c, l_k, and d_{app} from Table 3 and compared with the experimental data. Results are included in Table 3. In all cases, the theoretical value of R_h was smaller than the experimentally determined value; the discrepancy was greatest for Sample D.

An attempt was made to obtain SLS and DLS data on β(1–39) in 0.1% TFA. Scattered intensity was extremely weak, indicative of the substantially smaller size of the peptide in this solvent relative to that in PBSA. The particle size was still not measurable 1 week after sample preparation, indicating that no significant aggregation occurred in this solvent over time.

Phase separation

The onset of phase changes was determined by holding the light scattering cuvette to a light source and examining the sample by eye, and by gently tipping the cuvette to observe any flow. The time for visible precipitate formation of the samples depended on the initial stock solution. Sample A formed visible precipitates after 4 days. Sample B formed visible precipitates after 7 days. In contrast, no visible precipitates were observed in Samples C and D after 2 weeks. However, Samples C and D appeared viscous after 1 week, as determined by visual inspection. After a period of several weeks, a small amount of precipitate was eventually evident in Samples C and D.

DISCUSSION

Determination of the aggregation characteristics of Aβ might be important in understanding its physiological role. In work reported here, we used light scattering to obtain size and structural information of the fibril in solution. Preparation of samples from 0.1% TFA stock solutions was chosen for two reasons: (1) the low pH can potentially disaggregate any pre-aggregated material in the lyophilized peptide, hence leading to starting conditions that contain only monomeric peptide, and (2) 0.1% TFA is commonly used in 35% acetonitrile solutions for peptide purification and in stock solutions used in toxicity studies.

When dissolved in 0.1% TFA, with 0.1% TFA as a mobile phase, the peptide eluted on a size-exclusion column with residence time close to that of a monomer. DLS and SLS experiments confirmed that the peptide was unaggregated under these conditions. There was no detectable change in the tyrosine environment over time for the peptide dissolved in 0.1% TFA, as measured by fluorescence. In this solvent, our analysis indicated that the peptide contained some β-turn. Barrow et al. (1992) reported a greater (72%) fraction of random coil for β(1–39) in water buffered with 5 μM potassium phosphate at pH 2.8. The difference is possibly caused by a difference in the choice of reference spectra and the inclusion of β-turn in our analysis.

Upon dilution into phosphate buffer at neutral pH, β-sheet content increased concomitant with aggregation of the peptide. The secondary structure characteristics were very similar to those we reported previously for β(1–40) (Tomski and Murphy, 1992) and did not depend on the length of time that the sample was incubated in 0.1% TFA before dilution. Predissolving β(1–39) in 0.1% TFA before dilution into PBSA resulted in an initially smaller size (greater relaxation rate ⟨Γ⟩) as measured by DLS, when compared with dissolving lyophilized peptide directly into phosphate buffer. The size of the sample 20 min after preparation decreased with increasing pre-incubation time in 0.1% TFA. However, at only 20 min after sample preparation, $\langle R_h \rangle_{app}$ was 40 to 90 nm, which is substantially larger than the size expected for monomeric β(1–39). These results indicate that self-assembly of β(1–39) proceeds very rapidly upon introduction of a buffer at physiological pH and ionic strength.

SLS data taken 12 h after dilution of the peptide into PBSA provided a "snapshot" picture of the average fibril size and

architecture. At this time fibrils, with lengths on the order of 1 μm, contained an average of approximately 2000–6000 monomers. With increasing pre-incubation time in 0.1% TFA, fibrils of greater linear mass density, greater average molecular weight, and shorter contour length were formed. The molecular weight of Sample D was roughly 2 to 3 times that of Sample A, B, or C. The increase in linear density and corresponding increase in stiffness was largest for Sample D. These effects might be caused by lateral alignment of fibrils. Aligned filaments have been commonly reported in electron micrographs of amyloid fibrils (e.g., Narang, 1980; Merz et al., 1983; Halverson et al., 1990; Fraser et al., 1991). Tamarind seed polysaccharide has been reported to undergo a similar lateral aggregation process, resulting in an increase in stiffness (Lang et al., 1993). Alternatively, the changes in linear density and fibril flexibility might be caused by structural changes in the way that peptide monomers "pack" into fibrils.

The differences among the samples were not caused by changes in secondary structure or chemical composition, as described above. One possibility is that there are some stable preformed aggregates in the lyophilized peptide that are only slowly lost during incubation in TFA. Longer incubation times in TFA would lead to an increase in the concentration of monomers at the expense of these preformed aggregates, and changes in the average properties of the aggregated peptide. This hypothesis would be consistent with the smaller initial size with increasing pre-incubation time in TFA (Fig. 8).

The theoretical R_h was smaller than that actually measured. This could be caused by a number of effects. First, the theoretical R_h was calculated assuming that the diameter determined from the linear density corresponded to the hydrodynamically effective cross section. However, if the fibrils are loosely twisted or have frayed ends, the hydrodynamic cross section would be considerably greater, which would lead to a larger R_h. Second, effects of polydispersity were ignored in calculating the theoretical R_h.

Samples C and D remained soluble for several weeks, forming gels before precipitating. Physical gelation often occurs in stiff rod systems because of kinetic limitations (Tracy and Pecora, 1992). The increased rigidity of the fibrils, especially in Sample D, could lead to fibril entanglement and physical gelation. At 48 h, $\langle\Gamma\rangle$ for Sample C is similar to that for Sample D; this suggests that at longer times, these fibrils also aggregate laterally and increase in stiffness. Thus, the increased rigidity would lead to gelation for this sample. All samples eventually contained some insoluble material.

In interpreting the results from light scattering, three points must be addressed. First, in the analysis of SLS data using Eq. 2, the contribution of the second virial coefficient B was neglected. Assuming hard-core interactions only, the theoretical value of B for a rigid rod was calculated (Goinga and Pecora, 1991). From this, we estimated that the contribution from this term would lead to an increase in $\langle M\rangle_w$ of at most ~20% for Samples A and B, ~10% for Sample C, and ~5% for Sample D. Second, in determining the shape from the particle structure factor, we assumed that the fibrils are linear nonbranching chains and that interparticle effects are negligible. For many branched structures, an internal maximum in the Kratky plot appears (Burchard and Muller, 1980). This was not seen in our results. Furthermore, the theoretical and experimental values of radius of gyration agreed quite well, which would not be true for branched structures. For Samples A and B, the experimental data lie just slightly above the theoretical curve at intermediate q on a Kratky plot (Fig. 5). This could be because of a small degree of branching (Kajiwara and Ribeiro, 1974). Overall, however, the analysis of the fibrils as nonbranching chains appears justifiable. Third, the downward curvature at large q seen in Fig. 5 *D* could be caused by an increase in polydispersity rather than an increase in stiffness (Franken and Burchard, 1973). This is unlikely given the fact that the polydispersity index U is similar for all four samples.

To summarize, fibril dimensions, flexibility, and solubility can be altered by small changes in sample preparation method. Peptide self-assembly occurs very rapidly under our experimental conditions, and some forms of aggregated Aβ can remain soluble for considerable time periods. In assessing the role of aggregation state on the biological activity of Aβ, it is important not to assume that peptide solubility corresponds to unaggregated peptide; this distinction has not always been clearly made. Effects of sample preparation on fibril characteristics can be significant in altering the outcome of toxicity assessments of Aβ and need to be considered carefully when analyzing data on the biological activity of Aβ.

We thank Grayson Scott for assistance in obtaining the electron micrographs and S. Damodaran for providing access to a circular dichroism spectrometer. This work was supported by a grant from Alzheimer's Disease Research, a program of the American Health Assistance Foundation, and by a gift from the Robert M. Schiller Fund.

REFERENCES

Barrow, C. J., A. Yasuda, P. T. M. Kenny, and M. G. Zagorski. 1992. Solution conformations and aggregational properties of synthetic amyloid β-peptides of Alzheimer's disease. *J. Mol. Biol.* 225:1075–1093.

Benoit, H., and P. Doty. 1953. Light scattering from non-Gaussian chains. *J. Phys. Chem.* 57:958–963.

Burchard, W., and M. Muller. 1980. Statistics of branched polymers composed of rod substructures: a model for fibrin before clot formation. *Int. J. Biol. Macromol.* 2:225–234.

Burdick, D., B. Soreghan, M. Kwon, J. Kosmoski, M. Knauer, A. Henschen, J. Yates, C. Cotman, and C. Glabe. 1992. Assembly and aggregation properties of synthetic Alzheimer's βA/4 amyloid peptide analogs. *J. Biol. Chem.* 267:546–554.

Busciglio, J., A. Lorenzo, and B. A. Yankner. 1992. Methodological variables in the assessment of beta amyloid neurotoxicity. *Neurobiol. Aging.* 13:609–612.

Busciglio, J., J. Yeh, and B. A. Yankner. 1993. β-amyloid neurotoxicity in human cortical culture is not mediated by excitotoxins. *J. Neurochem.* 61:1565–1568.

Chang, C. T., C. C. Wu, and J. T. Yang. 1978. Circular dichroic analysis of protein conformation: inclusion of the β-turns. *Anal. Biochem.* 91:13–31.

Clemens, J. A., and D. T. Stephenson. 1992. Implants containing β-amyloid protein are not neurotoxic to young and old brain. *Neurobiol. Aging.* 13:581–586.

Cohn, E. F., and J. T. Edsall. 1943. Proteins, Amino Acids and Peptides. Reinhold Publishing Co., New York. 372.

Cowgill, R. W. 1976. Tyrosyl fluorescence in proteins and model peptides. *In* Biochemical fluorescence: Concepts. R. F. Chen and H. Edelhoch, editors. Marcel Dekker, New York. 441–486.

Emre, M., C. Geula, B. J. Ransil, and M.-M. Mesulam. 1992. The acute neurotoxicity and effects upon cholinergic axons of intracerebrally injected β-amyloid in the rat brain. *Neurobiol. Aging.* 13:553–559.

Franken, L., and W. Burchard. 1973. Application of the cascade theory to calculation of particle scattering factors of polydisperse systems of stiff chain. *Macromolecules.* 6:848–855.

Fraser, P. E., J. T. Nguyen, W. K. Surewicz, and D. A. Kirschner. 1991. pH-dependent structural transitions of Alzheimer amyloid peptides. *Biophys. J.* 60:1190–1201.

Frautschy, S., A. Baire, and G. M. Cole. 1991. Effects of injected Alzheimer β-amyloid cores in rat brain. *Proc. Natl. Acad. Sci. USA.* 88:8362–8366.

Games, D., K. M. Khan, F. G. Soriano, P. S. Keim, D. L. Davis, K. Bryant, and I. Lieberburg. 1992. Lack of Alzheimer pathology after β-amyloid protein injections in rat brain. *Neurobiol. Aging.* 13:569–576.

Glenner, G. G., and C. W. Wong. 1984. Alzheimer's disease: initial report of the purification and characterization of a novel cerebrovascular amyloid protein. *Biochem. Biophys. Res. Commun.* 120:885–890.

Goinga, H., and R. Pecora. 1991. Dynamics of low molecular weight DNA fragments in dilute and semidilute solutions. *Macromolecules.* 24: 6128–6138.

Haass, C., M. G. Schlossmacher, A. Y. Hung, C. Vigo-Pelfrey, A. Mellon, B. L. Ostaszewski, I. Lieberburg, E. H. Koo, D. Schenk, D. B. Teplow, and D. J. Selkoe. 1992. Amyloid β-peptide is produced by cultured cells during normal metabolism. *Nature.* 359:322–325.

Haass, C., and D. J. Selkoe. 1993. Cellular processing of β-amyloid precursor protein and the genesis of amyloid β-peptide. *Cell.* 75:1039–1042.

Halverson, K., P. E. Fraser, D. A. Kirschner, and P. T. Lansbury, Jr. 1990. Molecular determinants of amyloid deposition in Alzheimer's disease: conformational studies of synthetic β-protein fragments. *Biochemistry.* 29:2639–2644.

Hilbich, C., B. Kisters-Woike, J. Reed, C. L. Masters, and K. Beyreuther. 1991. Aggregation and secondary structure of synthetic amyloid βA4 peptides of Alzheimer's disease. *J. Mol. Biol.* 218:149–163.

Joachim, C. L., and D. J. Selkoe. 1992. The seminal role of β-amyloid in the pathogenesis of Alzheimer disease. *Alzheimer Dis. Assoc. Disord.* 6:7–34.

Jordano, J., J. L. Barbero, F. Montero, and L. Franco. 1983. Fluorescence of histones H1: a tyrosine-like fluorescence emission in *Ceratitis Capitata* H1 at neutral pH. *J. Biol. Chem.* 258:315–320.

Kajiwara, K., and C. A. M. Ribeiro. 1974. Dilute solution properties of randomly branched polymer systems. I. The particle scattering factor. *Macromolecules.* 7:121–128.

Kang, J., H.-G. Lemaire, A. Unterbeck, J. M. Salbaum, C. L. Masters, K.-H. Grzeschik, G. Multhaup, K. Beyreuther, and B. Muller-Hill. 1987. The precursor of Alzheimer's disease amyloid A4 protein resembles a cell-surface receptor. *Nature.* 325:733–736.

Klunk, W. E., J. W. Pettegrew, and D. J. Abraham. 1989. Quantitative evaluation of Congo red binding to amyloid-like proteins with a beta-pleated sheet conformation. *J. Histochem. Cytochem.* 37:1273–1281.

Koh, J.-Y., L. L. Yang, and C. W. Cotman. 1990. β-amyloid protein increases the vulnerability of cultured cortical neurons to excitotoxic damage. *Brain Res.* 533:315–320.

Kowall, N. W., M. F. Beal, J. Busciglio, L. K. Duffy, and B. A. Yankner. 1991. An in vivo model for the neurodegenerative effects of β amyloid and protection by substance P. *Proc. Natl. Acad. Sci. USA.* 88:7247–7251.

Kowall, N. W., A. C. McKee, B. A. Yankner, and M. F. Beal. 1992. In vivo neurotoxicity of beta-amyloid [β(1–40)] and the β(25–35) fragment. *Neurobiol. Aging.* 13:537–542.

Koyama, R. 1973. Light scattering of stiff chain polymers. *J. Phys. Soc. Jpn.* 34:1029–1038.

Kuntz, I. D., Jr., and W. Kauzmann. 1974. Hydration of proteins and polypeptides. *Adv. Prot. Chem.* 28:239–245.

Lang, P., K. Kajiwara, and W. Burchard. 1993. Investigations on the solution architecture of carboxylated tamarind seed polysaccharide by static and dynamic light scattering. *Macromolecules.* 26:3992–3998.

Loo, D. T., A. Copani, C. J. Pike, E. R. Whittemore, A. J. Walencewicz, and C. W. Cotman. 1993. Apoptosis is induced by β-amyloid in cultured central nervous system neurons. *Proc. Natl. Acad. Sci. USA.* 90: 7951–7955.

Masters, C. L., G. Simms, N. A. Weinman, G. Multhaup, B. L. McDonald, and K. Beyreuther. 1985. Amyloid plaque core proteins in Alzheimer disease and Down syndrome. *Proc. Natl. Acad. Sci. USA.* 82:4245–4249.

Mattson, M. P., B. Cheng, D. Davis, K. Bryant, I. Lieberburg, and R. E. Rydel. 1992. β-amyloid peptides destabilize calcium homeostasis and render human cortical neurons vulnerable to excitotoxicity. *J. Neurosci.* 12:376–389.

May, P. C., B. D. Gitter, D. C. Waters, L. K. Simmons, G. W. Becker, J. S. Small, and P. M. Robison. 1992. β-amyloid peptide in vitro toxicity: lot-to-lot variability. *Neurobiol. Aging.* 13:605–607.

Merz, P. A., H. M. Wisniewski, R. A. Somerville, S. A. Bobin, C. L. Masters, and K. Iqbal. 1983. Ultrastructural morphology of amyloid fibrils from neuritic and amyloid plaques. *Acta Neuropathol.* 60:113–124.

Narang, H. K. 1980. High-resolution electron microscopic analysis of the amyloid fibril in Alzheimer's diesase. *J. Neuropathol. Exp. Neurol.* 39: 621–631.

Pike, C. J., D. Burdick, A. J. Walencewicz, G. G. Glabe, and C. W. Cotman. 1993. Neurodegeneration induced by β-amyloid peptides in vitro: the role of peptide assembly state. *J. Neurosci.* 13:1676–1687.

Pike, C. J., A. J. Walencewicz, C. G. Glabe, and C. W. Cotman. 1991a. Aggregation-related toxicity of synthetic β-amyloid protein in hippocampal cultures. *Eur. J. Pharmacol.* 207:367–368.

Pike, C. J., A. J. Walencewicz, C. G. Glabe, and C. W. Cotman. 1991b. In vitro aging of β-amyloid protein causes peptide aggregation and neurotoxicity. *Brain Res.* 563:311–314.

Podlisny, M. B., D. T. Stephenson, M. P. Frosch, I. Lieberburg, J. A. Clemens, and D. J. Selkoe. 1992. Synthetic amyloid β-protein fails to produce specific neurotoxicity in monkey cerebral cortex. *Neurobiol. Aging.* 13:561–567.

Prelli, F., E. Castano, G. G. Glenner, and B. Frangione. 1988. Differences between vascular and plaque core amyloid in Alzheimer's disease. *J. Neurochem.* 51:648–651.

Rosenberg, R. N. 1993. A causal role for amyloid in Alzheimer's disease: the end of the beginning. *Neurology.* 43:851–856.

Schmidt, M., G. Paradossi, and W. Burchard. 1985. Remarks on the determination of chain stiffness from static scattering experiments. *Makromol. Chem.* 6:767–772.

Seubert, P., C. Vigo-Pelfrey, F. Esch, M. Lee, H. Dovey, D. Davis, S. Sinha, M. Schlossmacher, J. Whaley, C. Swindlehurst, R. McCormack, R. Wolfert, D. Selkoe, I. Lieberburg, and D. Schenk. 1992. Isolation and quantification of soluble Alzheimer's β-peptide from biological fluids. *Nature.* 359:325–327.

Shoji, M., T. E. Golde, J. Ghiso, T. T. Cheung, S. Estus, L. M. Shaffer, X.-D. Cai, C. M. McKay, R. Tintner, B. Frangione, S. G. Younkin. 1992. Production of the Alzheimer amyloid β-protein by normal proteolytic processing. *Science.* 258:126–129.

Simmons, L. K., P. C. May, K. J. Tomaselli, R. E. Rydel, K. S. Fuson, E. F. Brigham, S. Wright, I. Lieberburg, G. W. Becker, D. N. Brems, W. Li. 1994. Secondary structure of β-amyloid peptide correlates with toxicity in vitro. *Mol. Pharmacol.* 45:373–379.

Stein-Behrens, B., K. Adams, M. Yeh, and R. Sapolsky. 1992. Failure of beta-amyloid protein fragment 25–35 to cause hippocampal damage in the rat. *Neurobiol. Aging.* 13:577–579.

Tomski, S. J., and R. M. Murphy. 1992. Kinetics of aggregation of synthetic β-amyloid peptide. *Arch. Biochem. Biophys.* 294:630–638.

Tracy, M. A., and R. Pecora. 1992. Dynamics of rigid and semirigid rodlike polymers. *Annu. Rev. Phys. Chem.* 43:525–557.

Waite, J., G. M. Cole, S. A. Frautschy, D. J. Connor, and L. J. Thal. 1992. Solvent effects on beta protein toxicity in vivo. *Neurobiol. Aging.* 13:595–599.

Whitson, J. S., D. J. Selkoe, and C. W. Cotman. 1989. Amyloid β protein enhances the survival of hippocampal nuerons in vitro. *Science.* 243: 1488–1490.

Wong, C. W., V. Quaranta, and G. G. Glenner. 1985. Neuritic plaques and cerebrovascular amyloid in Alzheimer disease are antigenically related. *Proc. Natl. Acad. Sci. USA.* 82:8729–8732.

Yamakawa, H., and M. Fujii. 1973. Translational friction coefficient of wormlike chains. *Macromolecules.* 6:407–415.

Yankner, B. A., L. K. Duffy, and D. A. Kirschner. 1990. Neurotrophic and neurotoxic effects of amyloid β protein: reversal of tachykinin neuropeptides. *Science.* 250:279–282.